

Title: Heterogeneity and dynamics of cortical populations coding visual detection

Manuscript Length

Words in main body: 3016

Number of figures: 5

Authors and Affiliations

Authors: Jorrit S. Montijn¹, Pieter M. Goltstein^{1,2}, Cyriel M.A. Pennartz^{1,3}

1 Swammerdam Institute for Life Sciences, Center for Neuroscience, Faculty of Science, University of Amsterdam, the Netherlands

2 Max Planck Institute of Neurobiology, Martinsried, Germany

3 Research Priority Program Brain and Cognition, University of Amsterdam, the Netherlands

Summary

Previous studies have demonstrated the importance of the primary sensory cortex for the detection, discrimination and awareness of visual stimuli, but it is unknown how neuronal populations in this area process perceived and unperceived stimuli differently. Critical differences may reside in the mean strength of responses to visual stimuli, as reflected in bulk signals detectable in fMRI, EEG or MEG studies, or may be more subtly composed by differentiated activity of individual sensory neurons. Quantifying the heterogeneity of Ca²⁺ responses to visual stimuli recorded with *in vivo* 2-photon imaging, we found that visual perception correlates with activation of particular neural ensembles rather than overall response strength. Ensemble patterns recurred upon repetition of the same stimulus, but also showed a fleeting character across longer episodes. Contrary to models relying on temporally stable networks or bulk-signalling, these results suggest that perception critically depends on transient activation of selective and dynamic neuronal ensembles.

Introduction

Lesion studies in humans and animal species indicate the causal importance of the primary visual cortex (V1) in detection, discrimination and awareness of visual stimuli¹⁻³, and this role has been recently confirmed by direct optogenetic inhibition of mouse V1⁴. Visual perception has been proposed to arise from interactions between stimulus-specific processing in V1 and neural activity in higher visual and frontoparietal areas, involving both feedforward propagation of activity and recurrent, top-down feedback⁵⁻¹¹. Critical in unravelling neural correlates of vision is how perceived and unperceived stimuli are processed differently, especially when these stimuli are physically identical. For instance, it has been suggested that the intensity, duration and reproducibility of sensory neural activity may provide signatures critical for visual perception (e.g. ¹²⁻¹⁴). In addition, it has been proposed that neural activity in V1 does not correlate with visual perception because stimuli that were seen or not seen evoked similar V1 blood-oxygenation level dependent (BOLD) signals^{15,16}. However, the mean-field approach characteristic of fMRI, EEG and MEG studies leaves open the possibility that neural correlates of perception may be coded in more subtle ways that take into account the local differentiation present in populations of sensory neurons.

Such local, functional differentiation is widely supported by single- or multi-unit recording studies in V1 of animals trained to make perceptual decisions¹⁷⁻²³. However, because these studies have been usually limited to monitoring few neurons simultaneously, population-level processes underlying visual perception remain largely unknown. Various aspects of population coding in visual cortex have been studied, such as the importance of synchrony, noise correlations and sparseness for neural processing²⁴⁻³⁰, but their relevance for perception remains to be probed in paradigms where animals report behaviourally whether they have seen a stimulus or not. Therefore we investigated correlates of visual perception using two-photon calcium imaging of populations of >100 neurons in V1 of mice performing

a visual detection task. Our first aim was to examine whether visual detection correlates with the mean visual response strength of V1 neurons, or rather with the heterogeneity in their responses. Second, a widely held assumption in computational models of vision is that neurons in distributed architectures of lower and higher areas have relatively fixed roles in information coding, based on afferent and efferent connections that remain constant across short time scales (e.g.,^{31–36}). Working with well-trained animals, we asked whether the same ensemble activation patterns are generated reproducibly across trials that repeat the same stimulus presentation. We report that (i) visual perception does not correlate well with mean response strength, but strongly correlates with population heterogeneity, and (ii) ensemble activation patterns, although consistent at short time scales, have a fleeting nature along the course of a session of several hours.

Results

To investigate how ensembles of primary visual cortex (V1) neurons are involved in visual perception we trained mice to perform a go/no-go stimulus detection task (fig. 1a). After task acquisition, we performed two-photon calcium imaging in V1 contralateral to the visually stimulated eye (fig. 1b,d). During imaging, animals were awake, head-fixed and performed a detection task where they indicated by licking whether a square-wave drifting grating was presented. The stimulus duration was delimited by the onset of the licking response, with a maximum of 3.0 seconds for no response. To acquire a sufficient range of hit/miss ratios we presented stimuli with different luminance contrasts: 0.5%, 2%, 8%, 32% and 100% interleaved with 0% contrast probe trials.

To quantify behavioural performance during execution the task, we calculated the 95% confidence intervals (CI) of response proportions to probe trials and full contrast trials. All eight animals (see Online Methods for inclusion criteria) showed a significantly above-chance

visual detection of square-wave drifting gratings during the acquisition of neural data (fig. 1c) (non-overlapping Clopper-Pearson 95% CIs). Group-level analysis with a linear regression model showed that with higher stimulus contrasts behavioural response proportions increased (fig. 1e) (see Online Methods, $p < 0.001$) and mean reaction times decreased (fig. 1f) ($p < 0.005$).

Specific neural activity for hit trials

As a first approach to examine changes in population correlates of visual detection we investigated differences in mean activity levels between hit and miss trials. We calculated each neuron's preferred stimulus orientation (see Online Methods), and for each trial took the responses of only neurons that preferred the presented stimulus orientation (henceforth 'preferred population'). In fig. 2, all trials were grouped by stimulus contrast and behavioural response (hit/false-alarm ('response') or miss/correct-rejection ('no-response')), and the average preferred population response of each animal ($n=8$) was calculated per group. The mean response over animals increased with higher stimulus contrasts (fig. 2a; Extended Data Fig. 1-4). However, we did not find a significant difference between response and no-response trials for any individual contrast (false-discovery rate (FDR)-corrected paired t-test, $p > 0.05$ for all contrasts). When grouping the intermediate contrasts (0.5% – 32%), the data did show a difference between hit and miss trials (paired t-test, $p < 0.05$). This could indicate either that perception-related neural correlates in V1 are small, or that a simple enhancement of mean population activity is an index ill-suited to describe potentially strong, but more complex changes in neuronal population dynamics.

To compare the distributions of population activity over contrast and response type, we z-scored neuronal responses to stimuli per contrast and split them per behavioural response. If the hit-correlated enhancement in activity was caused by a general increase in

activation of all neurons (i.e., non-specific gain effect), then we should observe no difference in z-scored activity distributions between hit- and miss trials, because z-scoring will normalize any distribution's mean to 0 and its standard deviation to 1. However, if the effect is dependent on a change in skewness, which could indicate activity increases in specific subpopulations, then we should observe a difference in the probability densities between hit- and miss trials at specific locations of the distribution (e.g., heavier tail around higher z-scores for hit trials). We examined this for both hit (fig. 2c) and miss trials (fig. 2d) and observed a significant over-representation of highly active neurons in hit trials (fig. 2e). Thus, a specific subgroup of neurons contributes more to the mean increase in population activity on hit vs. miss trials than would be expected if this were a population-wide gain effect.

We next asked whether, given the same contrast level, hits are marked by higher population heterogeneity than misses. Several metrics aim to quantify this heterogeneity, such as the kurtosis of a distribution indicating the population sparseness³⁷. However, to properly estimate a distribution's kurtosis many data points are required, which could explain why experimental studies into population sparseness are rare and often require averaging over extended time periods (e.g.,³⁸, Extended Data Fig. 8). We developed an alternative measure of population heterogeneity (fig. 2f): by subtracting the z-scored response of each neuron from that of all other neurons at each time point, we obtained a Δz -score matrix where high values indicate a high dissimilarity in activation. Taking the mean over all pairwise Δz -score values provides a measure of population heterogeneity that can be computed over an arbitrarily small time interval. Similarly strongly activated as well as similarly weakly activated pairs of neurons will decrease heterogeneity, given in units of mean $\Delta\sigma$ (difference in standard deviations). By contrast, dissimilarly activated neuronal pairs (i.e., one strong, one weak) will increase it. Therefore population heterogeneity is a multi-faceted metric that incorporates both trial-by-trial fluctuations and intra-population differences.

We applied this novel metric to the population activity during hit and miss trials and found a much stronger correlation with behavioural stimulus detection (fig. 2b). Intermediate contrasts (0.5% – 32%) showed a highly significant increase in heterogeneity for hit trials (paired t-test, $p < 0.001$) and most also showed this on individual basis (FDR-corrected paired t-tests; 0.5%, $p = 0.424$; 2%, $p < 0.001$; 8%, $p < 0.05$; 32%, $p < 0.05$), but such modulations were absent for false alarm trials (no stimulus, 0% contrast, $p = 0.781$) or trials with 100% contrast ($p = 0.758$). We used a measure of effect size (Cohen's d) to quantify whether heterogeneity showed a stronger correlation with visual detection than dF/F_0 and observed a statistically significant difference (dF/F_0 , mean $d = 0.100$; heterogeneity, mean $d = 0.227$; paired t-test, $p < 0.05$). These results show that heterogeneity is better able to capture V1 population correlates of visual detection than is mean response strength. They also suggest that changes in V1 population dynamics that determine the accuracy of visual task performance are more related to preferential activation of certain neuronal subpopulations than to overall increases in mean activation.

However, changes in population heterogeneity might be uncorrelated with the fidelity of the population code representing visual stimulus properties in. To address this, we used a Bayesian maximum-likelihood decoder that extracts the orientation and contrast of presented stimuli from V1 population activity (Online Methods and ²⁶ for more details). We compared the decoder's accuracy between hit and miss trials and found that stimulus orientation and contrast were on average better decodable for hit trials (fig. 3a; paired t-test, $p < 0.05$). V1 population activity is therefore in fact representing stimulus features with higher fidelity when the animal makes a correct response.

The behavioural task was stimulus detection *per se*, with stimulus contrast and orientation being irrelevant for the animal. We therefore also decoded the presence or absence of a visual stimulus from the population response rather than its features by training the

algorithm only on 0% vs. 100% contrast stimuli, and regardless of orientation (fig. 3e). Decoding performance was higher for behaviourally correct detection trials (paired t-test, hit vs. miss, $p < 0.05$) and the performance as a function of contrast was strikingly similar to the animals' actual behavioural performance (paired t-test shuffled vs. non-shuffled, $p < 0.001$) (fig. 3f). Thus the animals performed similarly to an ideal Bayesian observer situated at the output of V1: much of the variability in behavioural performance can be attributed to uncertainty in V1 population activity.

So far we have shown that both heterogeneity and accurate decoding correlate with correct stimulus detection, but not whether heterogeneity correlates with accurate decoding. We therefore used a similar algorithm to infer the presented stimulus orientation (fig. 3b). The accuracy of decoding did not depend on the mean population dF/F_0 (fig. 3c) (paired t-test, $p = 0.669$), but we did observe a beneficial effect of population heterogeneity on accuracy (fig. 3d) (paired t-test, $p < 0.05$).

Heterogeneity predicts reaction time

Our observations suggest that not a gain increase in population activity, but rather the strong responses of a specific subset of neurons determine both the coding fidelity and behavioural accuracy. Behavioural reaction times are often used as proxies for salience, attention and readiness³⁹, so we expected to find similar dissociations for fast/slow responses as for hit/miss trials. We performed linear regressions per animal for dF/F_0 (fig. 4a) and heterogeneity (fig. 4b) as a function of reaction time. Similarly to hit/miss differences, dF/F_0 was not significantly associated with behavioural performance (regression slopes vs. 0, FDR-corrected one-sample t-test, n.s.) nor were z-scored activity, population variance and sparseness (Extended Data Fig. 8), but heterogeneity was strongly and inversely correlated with reaction

time ($p < 0.001$) and explained significantly more reaction-time dependent variance in the data than the four other measures (Extended Data Fig. 8f).

During higher levels of arousal, it has been observed that neuronal activation is more desynchronized^{22,38}. This led us to hypothesize that high heterogeneity of V1 populations may reflect a brain state that is conducive to stimulus perception. If correct, heterogeneity immediately prior to stimulus presentation should be predictive of reaction time. To test this, we split all hit trials into the slowest 50% and fastest 50% per contrast (see fig. 4c,d for an example) and calculated a Measure of Predictability of slow vs. fast responses based on the three seconds preceding stimulus presentation (fig. 4e-g; Extended Data Fig. 5). Using pre-stimulus-onset heterogeneity, fast response trials were highly predictable (FDR-corrected one-sample t-tests, $p < 0.001$), while slow vs. miss trials were not ($p = 0.799$). Behavioural responses were not predictable based on $dF/F0$ (slow-miss, $p = 0.157$; slow-fast, $p = 0.811$; fast-miss, $p = 0.924$), and the difference in predictability between heterogeneity and $dF/F0$ was significant for slow-fast ($p < 0.01$) and fast-miss ($p < 0.05$), but not for slow-miss ($p = 0.477$) trials.

Temporal consistency of the population code

So far we have mainly addressed static differences in population activity structure correlating with behavioural responses. However, population codes can show complex temporal properties, such as transient formation of assemblies^{24,40}. After confirming the stability of our recordings to avoid potential confounds (Extended Data Fig. 9), we addressed whether such temporal population structures might offer additional insight in neural mechanisms of visual detection. First we investigated whether the observed increases in population $dF/F0$ associated with accurate task performance are caused by the same subset of neurons returning on each trial (i.e., dynamic ensemble reoccurrences) or different subsets (i.e., a temporally random

population code). We studied the consistency of the 33% neurons that showed highest increases in dF/F_0 during hit trials, compared over contrasts (Extended Data Fig. 6). If visual detection would rely on a specific, anatomically defined subset of neurons, then this consistency should be close to 1.0, whereas if it is mediated by a group of neurons randomly selected on each trial, it should be close to 0.0. Our analysis shows that this consistency is low (correlation coefficient $r=0.057$), but significantly different from 0 (one-sample t-test, $p<0.05$) (fig. 5a). This indicates a predisposition of a subset of neurons to be involved in activity increases during hit trials, but also highlights the temporally dynamic nature of population responses.

As the above analysis may have a limited sensitivity in detecting reproducible ensemble activations across trials, we used a more generally applicable ensemble consistency index. For each animal we computed all pairwise neuronal response correlations per complete stimulus repetition (i.e., signal correlations) (fig. 5b). Next, we computed the correlation between this population response structure for a given trial and all other stimulus repetitions (fig. 5c). We then plotted the inter-repetition correlation (ensemble consistency index) versus inter-repetition time and performed a linear regression. Our analysis shows a significant intercept (ensemble consistency above zero, $\text{mean}=0.20$) and a decline over time (one-sample t-tests, both $p<0.05$) (fig. 5d). Because these consistency values cannot fully account for the population activity structure, we interpret the reoccurrences as happening against a background of dynamic activity.

Next we investigated how these reoccurrences depended on reaction time. We again split the data into miss, fast and slow response trials, and computed the inter-trial correlations separately for preferred and non-preferred neuronal populations. For fast response trials, the preferred population showed significant pattern reoccurrences (FDR-corrected one-sample t-test, $p<0.05$) that were not present for miss ($p=0.791$) or slow ($p=0.303$) response trials (fig.

5e), nor for any response type in the non-preferred population ($p=0.356$ for miss, $p=0.809$ for fast and $p=0.618$ for slow trials) (fig. 5f).

Overall we conclude that visual detection involves some V1 ensembles more than others and that these ensembles are of a fleeting nature. The strong correlation between behaviourally reported percepts and population heterogeneity (fig. 2b,4b,e) is only partly reflected in consistent reoccurrences of anatomically defined ensembles (fig. 5a,e). Therefore the source of strong population heterogeneity and its relation to behavioural output does not reside in a particular set of neurons (Extended Data Fig. 7). Rather, the high heterogeneity characteristic for hit trials must result from the temporally dynamic activity pattern of a population as a whole: during epochs of high heterogeneity the relative difference in activity between subsets of neurons increases, whereas between different epochs these subsets show decreasing reoccurrence probabilities.

Discussion

We found that behavioural stimulus detection correlates with selective, stimulus-induced activation of particular neural ensembles rather than overall response strength. Using a novel measure of population heterogeneity we show that the differentiation in activation of these ensembles predicts visual detection and is associated with an increased accuracy of stimulus feature representation by the population. High heterogeneity prior to stimuli correlated with fast hit responses, indicating that stimulus-induced assembly formation is likely gated by arousal mechanisms. Neuronal ensembles that are preferentially active during accurate task performance reoccur upon repetition of the same stimulus, but also show a fleeting character, showing that these ensembles are only stable on short time scales. Taken together, these results suggest that neural processing of information related to visual perception critically

depends on transient activation of selective, temporally dynamic neuronal ensembles, rather than on temporally stable ensembles or on modulation of population activity as a whole.

It is interesting to compare our results on heterogeneity with studies reporting that sparseness in L2/3 populations of rodent V1 is high⁴¹, depends on cortical state and improves neural discriminability of passively presented natural scenes³⁸. These properties have been hypothesized to be important for visual perception, but so far no studies have shown that they are relevant for behaviourally reported percepts. Here, we show that population heterogeneity is strongly correlated with behavioural stimulus detection and that it accurately predicts correct behavioural performance. Our results imply that neurophysiological measures dependent on population averages (i.e., multi-unit activity (MUA), electro-encephalograms (EEG) and functional magnetic resonance imaging (fMRI)) may underestimate the correlation between visual perception and V1 activity not because those correlates are weak, but rather because the assumption of population response homogeneity is violated especially during active processing of visual information. Our results support contrast-sensitive changes in mean population activity during visual task performance (fig. 2a), but stress the importance of population recordings with single-cell resolution (fig. 2b).

Our second main result is the relatively fast decay of ensemble consistency across stimulus repetitions. This provides some constraints on how population heterogeneity and transient ensemble formation are modulated at a neurophysiological level. Neuromodulators such as acetylcholine (ACh) and noradrenaline are correlated with attention and arousal, and may influence cortical population dynamics⁴²⁻⁴⁴, such that during prolonged task epochs the brain state gradually drifts away from its initial condition and correspondingly, away from the initially active ensembles. For instance, ACh has been observed to influence burst spiking, membrane fluctuations and cortical oscillations; processes involved in modulating competitive inhibition effects within neuronal populations⁴⁵⁻⁴⁷. If heterogeneity in a

recurrently connected V1 population is in part determined through suppression of the most weakly by the most strongly stimulus-driven neurons, then behaviourally correlated heterogeneity enhancements may be another facet of arousal-related modulations of stimulus-evoked population activity.

Online Methods

Animals and surgery

All experimental procedures were conducted with approval of the animal ethics committee of the University of Amsterdam (cf. ^{26,48}). Experiments were performed on eight adult, male wild-type C57BL/6 mice (Harlan), 128-164 days old at the day of calcium imaging (29.1 – 32.7 grams). Prior to the imaging experiment, all animals were surgically fitted with a head-bar implant and trained head-fixed for up to three months to perform a visual go/no-go detection task. At the day of the imaging experiment, we performed intrinsic signal imaging to define the area corresponding to the retinotopic region in V1 responsive to the visual stimulus. We performed a small (1.5-2.0mm) craniotomy at that location and used multi cell bolus loading with Oregon Green BAPTA-1 AM to record calcium transients and Sulforhodamine-101 to label astrocytes (see Supplementary Methods for more detailed information about surgical procedures and behavioural training).

Visual stimulation

All visual stimulation was performed on a 15 inch TFT screen with a refresh rate of 60Hz positioned at 16 cm from the mouse's eye, which was controlled by MATLAB using the PsychToolbox extension. Stimuli consisted of sequences of eight different directions of square-wave drifting gratings that were monocularly presented in randomized order. Visual

stimulus duration started at infinite during the initial training phase and was gradually reduced to a maximum duration of three seconds for the final task stage. Stimuli were alternated by a blank inter-trial interval of variable duration (minimum of 10-12 seconds) during which an isoluminant grey screen was presented. Visual drifting gratings (diameter 60 retinal degrees, spatial frequency 0.05 cycles/degree, temporal frequency 1 Hz) were presented within a circular cosine-ramped window to avoid edge effects at the border of the circular window. A field-programmable gate array (FPGA, OpalKelly XEM6001) was connected to the microscope and behavioural setup and interfaced with the visual stimulus presentation computer to synchronize the timing of visual stimulation with the microscope frame acquisition and behavioural setups.

Calcium imaging recordings and final task parameters

Dual-channel two-photon imaging recordings (filtered at 500-550nm for OGB and 565-605nm for SR101; see fig. 1b) with a 512 x 512 pixel frame size were performed at a sampling frequency of 25.4 Hz. We used an *in vivo* two-photon laser scanning microscopy setup (modified Leica SP5 confocal system) with a Spectra-Physics Mai-Tai HP laser set at a wavelength of 810 nm to simultaneously excite OGB and SR101 molecules, as previously described²⁶. During data acquisition mice were performing a go/no-go stimulus detection task. Stimulus parameters were equal to those described above for the final stage of behavioural training (stage 5), except that we now also varied the contrast of the drifting grating (0%, 0.5%, 2%, 8%, 32% and 100%). Responses to 0% contrast probe trials were not rewarded, but responses to all other contrasts were. A complete set of visual stimuli therefore consisted of 48 trials (6 contrasts times 8 directions). The order of presentation of these 48 trials was randomized independently for each repetition block. After the experiment was completed we tested for statistically significant stimulus detection performance by calculating

the 95% binomial confidence intervals (CIs) of response proportion to 100% and 0% contrast stimuli using the Clopper-Pearson (CP) method. Of the 10 animals from which we recorded calcium imaging data during task performance, one was rejected because of excessive variability in responses due to brain movement, and one was rejected due to insufficient discriminability between probe trials and visual stimulation trials (overlapping CIs). All data we present in this paper are from the remaining eight animals.

Eye tracking

We recorded eye movements during the entirety of the calcium imaging experiment to be able to correct for possible contamination of our results by excessive blinking and/or saccades. For this purpose we placed a near-infrared light sensitive camera (JAI CV-A50IR-C Monochrome 1/2" IT CCD Camera) with a large-aperture narrow-field lens (50 mm EFL, f/2.8) above the visual stimulation screen directed at the mouse's visually stimulated eye. Images were acquired at 25 Hz and pupil tracking was performed offline using custom-written MATLAB scripts.

Data preprocessing

After a recording was completed small x-y drifts were corrected offline with an image registration algorithm⁴⁹. To retrieve dF/F_0 values from the recordings, regions of interest (ROIs; neurons, astrocytes and blood vessels) were determined semi-automatically using custom-made MATLAB software for each repetition block separately. For these ROIs we subsequently calculated dF/F_0 values as previously described²⁶: For each image frame i a single dF_i/F_{0i} value was obtained for each neuron by calculating the baseline fluorescence (F_{0i}), taken as the mean of the lowest 50% during a 30-second window surrounding image

frame i . dF_i is defined as the difference between the fluorescence for that neuron in the given frame and the sliding baseline fluorescence ($dF_i = F_i - F_{0i}$)²⁶. The mean number of simultaneously recorded neurons/session was 92.6 (range: 68 – 130 (sd: 19.0) neurons). After this initial analysis all neurons were tested on consistency for preferred stimulus orientation and any neurons that showed inconsistencies over different repetition blocks were rejected from further analysis (mean number of consistently tuned neurons per animal was 66.3 +/- 18.6 (70.8% +/- 7.75% of all neurons) (mean +/- sd)). Unless otherwise specified, all analyses shown in this paper are based on across-animal meta statistics based on a set of 8 independent data points (one data point / animal) and all multiple comparison t-test p-values were adjusted by the Benjamini & Hochberg False-Discovery Rate correction procedure and were deemed significant if the resultant p-value was lower than 0.05. For quantification and control procedures related to z-drift and recording stability, see Supplementary Methods.

Calculation of preferred stimulus orientation

We presented eight directions of visual drifting gratings and calculated the preferred stimulus orientation of all neurons by summing opposite directions as belonging to the same stimulus type, because the vast majority of mouse V1 neurons is tuned sharply to an axis of movement, but much less so to a specific direction within that axis (i.e., most neurons are strongly orientation-tuned, but less direction-tuned (e.g.,⁵⁰). For these four orientations we took each neuron's mean response over all trials, and defined its preferred orientation as the stimulus that caused the highest mean dF/F_0 value.

Z-scored distribution comparison

To compare the shapes of neuronal response distributions of contrasts and quantify the difference in shapes between hit and miss trials, we divided each animal's data set into neuronal responses for the different contrasts. Next, we z-scored these responses separately for each contrast (c) and behavioural response (r), while grouping different orientations (θ), neurons (n) and repetitions (i):

$$Z_{c,\theta,r,n,i} = (R_{c,\theta,r,n,i} - \hat{R}_{c,r})/\sigma_{c,r} \quad (\text{eq. 1})$$

Here, $\hat{R}_{c,r}$ and $\sigma_{c,r}$ are the mean and standard deviation of the population response for contrast c and behavioural response type r (response/no response). Next we calculated the probability density functions of neuronal responses in bins of 0.1σ between -1.0σ and $+2.0 \sigma$ for each contrast and response type, yielding a 6×31 (contrast x z-scored bin) matrix for hit (H) and miss (M) trials each (fig. 2c,d). Next, we took the mean over animals of probability density matrices and calculated the element-wise hit/miss ratio of probability densities:

$$R_{z,c} = H_{z,c} / (H_{z,c} + M_{z,c}), \quad (\text{eq. 2})$$

Where \mathbf{R} is the ratio matrix, \mathbf{H} the hit-response matrix, \mathbf{M} the miss-response matrix, z the z-scored bin and c stimulus contrast. Statistical significance was quantified by performing a shuffling procedure (1000 iterations) where for each iteration per animal all probability-density ratio bins were randomly rearranged and the mean bin-wise ratio was calculated over animals. After shuffling, we calculated the 95% confidence interval (CI) per bin and defined bins as statistically significant when their real means were above the shuffled 95% CI (fig. 2e).

Heterogeneity calculation

We calculated population activity heterogeneity as follows (see also fig. 2f). For each independent data source i (i.e., a neuron) that provides a certain measurement R at each time point τ (i.e., mean activity at a single trial, or dF/F_0 at a single frame), we first z-scored the responses of i over all time points T :

$$Z_{i,t} = (R_{i,t} - \mu_i) / \sigma_i \quad (\text{eq. 3})$$

\mathbf{Z} is therefore a matrix containing n (number of neurons) by T (time points) measurements of standard deviations (σ) from the mean (μ). Next, for each time point t we calculated the pairwise distance (in standard deviations) from each independent source to each other independent source (pairwise neuronal $\Delta\sigma$): we repeated the vector \mathbf{z}_t over its singular dimension n times, where n is the number of elements in \mathbf{z}_t (yielding a square matrix), subtracted this matrix from its own transpose \mathbf{z}_t^T , and took the absolute of the result, giving the heterogeneity matrix \mathbf{H}_t :

$$\mathbf{H}_t = | \mathbf{z}_t - \mathbf{z}_t^T | \quad (\text{eq. 4})$$

To get a single measure of population heterogeneity per time point (h_t), we next took the mean of all z-score distances between neuronal pairs (i,j) in the heterogeneity matrix; this provides a measure of the mean distance in activation levels within our population at a single time point t :

$$h_t = \sum_{i=[1 \dots n-1]} \sum_{j=[i \dots n]} (H_{t,i,j}) / ((n \cdot (n - 1)) / 2) \quad (\text{eq. 5})$$

Effect size mean population dF/F_0 and heterogeneity

We used a measure of effect size using Cohen's d to quantify which metric (mean dF/F0 or heterogeneity) showed a stronger correlation with visual detection. We calculated for both metrics per animal the effect size for all intermediate contrasts (0.5% – 32%) between hit and miss trials and took the mean over these four values, yielding a mean hit/miss effect size for dF/F0 and heterogeneity per animal. This allowed us to perform a paired t-test between the dF/F0 effect sizes and heterogeneity effect sizes to test for statistical significance. Cohen's d is defined as the difference between the two means (hit; μ_h , miss; μ_m) divided by the pooled standard deviation for the data;

$$d = (\mu_h - \mu_m) / \sigma_p, \quad (\text{eq. 6})$$

where σ_p is defined as

$$\sigma_p = \sqrt{[(n_h - 1) * \text{var}_h + (n_m - 1) * \text{var}_m] / (n_h + n_m - 2)} \quad (\text{eq. 7})$$

Stimulus feature decoding

To address whether visual stimulus features (i.e., orientation and contrast) were more accurately represented by neuronal population activity during correct vs. incorrect behavioral performance, we used a Bayesian maximum-likelihood decoder to extract those features from the population activity (for a more complete description, see ²⁶). We defined all combinations of orientations and contrasts as different stimulus types, yielding a total of 21 different stimulus types (four orientations times five contrasts plus probe trials). Next, we performed a leave-one-out cross-validated decoding procedure for all trials and calculated the mean percentage correct decoding trials for hits and misses per stimulus type; then we averaged the percentage correct over stimulus types, yielding an accuracy per animal for hit and miss trials. We tested for a statistical difference between hits and misses with a paired t-test over animals (fig. 3a).

Decoding of stimulus presence

To ascertain the performance of a decoder on the same task as we required the mouse to perform, we created an algorithm that calculated the probability of a stimulus being present. Therefore, we used a similar maximum-likelihood decoder as above, but now defined only two stimulus categories based on the population activity during 0% contrast (probe) trials and 100% contrast stimulus trials. For each trial, we used only the preferred neuronal population for that trial's stimulus orientation to calculate the probability of stimulus presence. If the to-be-decoded trial contrast was 0% or 100%, we recalculated the likelihood to retain cross-validation and avoid inclusion of the decoded trials in the likelihood. If the trial's contrast was 0.5% - 32%, automatic cross-validation was guaranteed, because the likelihood was only based on 0% and 100% contrast responses. After decoding stimulus presence for all trials, we split the trials into response and no-response and calculated the percentage for which the decoder indicated a stimulus was present per response type and contrast, averaging over repetitions and orientations. This yielded two curves per animal (see fig. 3e). We tested for statistically significant differences between response and no-response trials by performing a paired t-test over animals on the intermediate contrasts (0.5-32%).

Furthermore, we quantified the similarity of our decoder's performance to the animal's performance in the visual stimulus detection task, by calculating the similarity per animal of its actual behavioural performance to the decoder's performance (Pearson correlation over contrasts). We compared this value to the similarity obtained with a bootstrapped shuffling procedure (1000 iterations). Here, we shuffled the animal's behavioural and decoder performance over contrasts, recalculated the similarity index and took the mean over all iterations as the resultant shuffled similarity. To test for statistical significance, we performed a paired t-test over animals between the shuffled and real similarities (fig. 3f).

Orientation decoding

Next we addressed whether the orientation information contained in the population responses was dependent on the mean $dF/F0$ and heterogeneity during stimulus presentation. We decoded the presented stimulus orientation for each contrast separately (i.e., 100% contrast trials based on likelihood from 100% contrast trials, etc.) by a leave-one-out cross-validation and afterwards split all trials into correctly and incorrectly decoded (fig. 3b). To quantify the dependence of decoding accuracy on $dF/F0$ during stimulus presentation, we took for each contrast the trials with highest and lowest 50% of $dF/F0$ and calculated the mean decoding accuracy for both groups (high and low activity). Next, we took the mean for these groups over contrasts per animal and calculated a percentage decoding accuracy increase for the highest vs. lowest 50% $dF/F0$ trials (see fig. 3c). To test for statistical significance, we performed a one-sample t-test of the percentage increase values over animals. For heterogeneity, we performed the same steps and performed a t-test vs. 0% increase (fig. 3d).

Behavioural response predictability

We analysed the predictability of behavioural responses before they occurred based on either the mean population $dF/F0$ response or population heterogeneity between 3 and 0 seconds before stimulus onset. Hit trials were split into the 50% fastest and 50% slowest reaction times per contrast per animal and then averaged over contrasts, yielding 6 data points per animal: the mean pre-stimulus population $dF/F0$ and mean population heterogeneity preceding fast, slow and miss trials. We then quantified the consistency of differences over animals by calculating the distance of these points per animal to the mean of their own

response group and the other two. We defined the predictability metric per point i (animal) for two response types $r1$ and $r2$ (i.e., two types out of fast, slow or miss) as:

$$\delta_{r1,r2,i} = \frac{\|d(i_{r1}, \mu_{r2})\|}{(\|d(i_{r1}, \mu_{r2})\| + \|d(i_{r1}, \mu_{r1}^{-i})\|)}, \quad (\text{eq. 8})$$

where $\|d\|$ is the absolute Euclidian distance (vector magnitude), μ_r is the mean location of \mathbf{I}_r – where \mathbf{I}_r is the group of points for response r – and μ_r^{-i} indicates the mean location of \mathbf{I}_r without point i . This analysis yields a vector $\delta_{r1,r2}$; the separability between response type $r1$ and $r2$. Random placement would lead to a separability of $\delta = 0.5$, so we quantified statistically significant predictability of responses by performing FDR-corrected one-sampled t-tests (vs. 0.5) for each separability vector and both neuronal population metrics (heterogeneity and mean dF/F0). We also tested whether the separability was higher for heterogeneity or dF/F0 by performing FDR-corrected paired t-tests between dF/F0 and heterogeneity separability vectors for the same response type comparisons (fig. 4e). To further validate our results on a single trial basis, we performed additional analyses explained in the Supplementary Methods.

Consistency of hit-correlated response enhancement

To test the hypothesis that V1 neural correlates of stimulus detection are dependent only on a small subset of neurons, we analysed the consistency of the 33% highest hit-correlated neurons per contrast. First we split the dataset into different contrast trials (excluding probes) and ordered all neurons by the difference in dF/F0 they showed between response and no-response trials (Extended Data Fig. 6). Then we took the 33% neurons with the highest increase in dF/F0 from miss to hit trials per contrast and calculated a correlation matrix between contrasts of which neurons belonged to the highest 33% (neurons x contrasts; see fig. 5a). Finally, we took the average of these inter-contrast correlations over animals and

performed a one-sample t-test of the average pairwise contrast correlations to test for statistical significance.

Consistency of population code over time

The aforementioned consistency of hit-correlated enhancement takes into account only the identity of an arbitrarily defined subgroup of neurons that increases the dF/F_0 responses during hit trials more than others. Therefore a more general ensemble consistency analysis might prove to be more sensitive to stimulus-induced reoccurrences in population activity structure. We computed a pairwise neuronal Pearson correlation matrix per stimulus repetition of neuronal responses to the different stimuli (signal correlations) (fig. 5b), and then computed the correlation between the population activity structure during these stimulus repetitions (fig. 5c). We took all inter-repetition correlation values and plotted them versus the time elapsed between these repetitions. Next we performed a linear regression, yielding an intercept and slope per animal. Statistical significance was evaluated by performing a one-sample t-test of the slopes and intercepts (fig. 5d).

Subpopulation reoccurrences

A further question regarding population code stability is whether the inter-trial correlation of population activity is different depending on the behavioural performance of the animal. To address this question we again separated fast, slow and miss trials and for each stimulus orientation calculated the correlation of the dF/F_0 response vector between pairs of trials with the same behavioural response. We separated the neuronal responses for that orientation's preferred and non-preferred population of neurons, also to address whether reoccurrences might be restricted to the preferred population or would also occur in the non-preferred

population (fig. 5e,f). To test for statistically significant reoccurrences, we performed FDR-corrected one-sample t-tests versus 0 correlation on the observed mean inter-trial correlations over animals for the different response types and the two neuronal population types.

References

1. Lashley, K. S. Studies of cerebral function in learning XII. Loss of the maze habit after occipital lesions in blind rats. *J. Comp. Neurol.* **79**, 431–462 (1943).
2. Weiskrantz, L., Warrington, E. K., Sanders, M. D. & Marshall, J. Visual Capacity in the Hemianopic Field Following a Restricted Occipital Ablation. *Brain* **97**, 709–728 (1974).
3. Weiskrantz, L. Blindsight revisited. *Curr. Opin. Neurobiol.* **6**, 215–220 (1996).
4. Glickfeld, L. L., Histed, M. H. & Maunsell, J. H. R. Mouse Primary Visual Cortex Is Used to Detect Both Orientation and Contrast Changes. *J. Neurosci.* **33**, 19416–19422 (2013).
5. VanRullen, R. & Koch, C. Is perception discrete or continuous? *Trends Cogn. Sci.* **7**, 207–213 (2003).
6. Rees, G., Kreiman, G. & Koch, C. Neural correlates of consciousness in humans. *Nat. Rev. Neurosci.* **3**, 261–270 (2002).
7. Haynes, J.-D., Driver, J. & Rees, G. Visibility Reflects Dynamic Changes of Effective Connectivity between V1 and Fusiform Cortex. *Neuron* **46**, 811–821 (2005).
8. Lamme, V. A. F., Supèr, H., Landman, R., Roelfsema, P. R. & Spekreijse, H. The role of primary visual cortex (V1) in visual awareness. *Vision Res.* **40**, 1507–1521 (2000).
9. Shadlen, M. N. & Newsome, W. T. Motion perception: seeing and deciding. *Proc. Natl. Acad. Sci.* **93**, 628–633 (1996).
10. Britten, K. H. & van Wezel, R. J. A. Electrical microstimulation of cortical area MST biases heading perception in monkeys. *Nat. Neurosci.* **1**, 59–63 (1998).
11. Dehaene, S. & Changeux, J.-P. Experimental and Theoretical Approaches to Conscious Processing. *Neuron* **70**, 200–227 (2011).
12. Rees, G. Neural correlates of the contents of visual awareness in humans. *Philos. Trans. R. Soc. B Biol. Sci.* **362**, 877–886 (2007).

13. Moutoussis, K. & Zeki, S. The relationship between cortical activation and perception investigated with invisible stimuli. *Proc. Natl. Acad. Sci.* **99**, 9527–9532 (2002).
14. Schurger, A., Pereira, F., Treisman, A. & Cohen, J. D. Reproducibility Distinguishes Conscious from Nonconscious Neural Representations. *Science* **327**, 97–99 (2010).
15. Vuilleumier, P. *et al.* Neural fate of seen and unseen faces in visuospatial neglect: A combined event-related functional MRI and event-related potential study. *Proc. Natl. Acad. Sci.* **98**, 3495–3500 (2001).
16. Rees, G. *et al.* Unconscious activation of visual cortex in the damaged right hemisphere of a parietal patient with extinction. *Brain* **123**, 1624–1633 (2000).
17. Posner, M. I. & Gilbert, C. D. Attention and primary visual cortex. *Proc. Natl. Acad. Sci.* **96**, 2585–2587 (1999).
18. McAdams, C. J. & Maunsell, J. H. R. Effects of Attention on Orientation-Tuning Functions of Single Neurons in Macaque Cortical Area V4. *J. Neurosci.* **19**, 431–441 (1999).
19. Womelsdorf, T., Fries, P., Mitra, P. P. & Desimone, R. Gamma-band synchronization in visual cortex predicts speed of change detection. *Nature* **439**, 733–736 (2005).
20. Bosman, C. A. *et al.* Attentional Stimulus Selection through Selective Synchronization between Monkey Visual Areas. *Neuron* **75**, 875–888 (2012).
21. Mitchell, J. F., Sundberg, K. A. & Reynolds, J. H. Spatial Attention Decorrelates Intrinsic Activity Fluctuations in Macaque Area V4. *Neuron* **63**, 879–888 (2009).
22. Cohen, M. R. & Maunsell, J. H. R. Attention improves performance primarily by reducing interneuronal correlations. *Nat. Neurosci.* **12**, 1594–1600 (2009).
23. Logothetis, N. K., Pauls, J. & Poggio, T. Shape representation in the inferior temporal cortex of monkeys. *Curr. Biol.* **5**, 552–563 (1995).

24. Luczak, A., Bartho, P. & Harris, K. D. Gating of Sensory Input by Spontaneous Cortical Activity. *J. Neurosci.* **33**, 1684–1695 (2013).
25. Vinje, W. E. & Gallant, J. L. Sparse Coding and Decorrelation in Primary Visual Cortex During Natural Vision. *Science* **287**, 1273–1276 (2000).
26. Montijn, J. S., Vinck, M. & Pennartz, C. M. A. Population coding in mouse visual cortex: response reliability and dissociability of stimulus tuning and noise correlation. *Front. Comput. Neurosci.* **8**, 58 (2014).
27. Olshausen, B. A. & Field, D. J. Sparse coding with an overcomplete basis set: A strategy employed by VI? *Vision Res.* **37**, 3311–3326 (1997).
28. Ma, W. J., Beck, J. M., Latham, P. E. & Pouget, A. Bayesian inference with probabilistic population codes. *Nat. Neurosci.* **9**, 1432–1438 (2006).
29. Averbeck, B. B., Latham, P. E. & Pouget, A. Neural correlations, population coding and computation. *Nat. Rev. Neurosci.* **7**, 358–366 (2006).
30. Benucci, A., Saleem, A. B. & Carandini, M. Adaptation maintains population homeostasis in primary visual cortex. *Nat. Neurosci.* **16**, 724–729 (2013).
31. Jones, J. P. & Palmer, L. A. An evaluation of the two-dimensional Gabor filter model of simple receptive fields in cat striate cortex. *J. Neurophysiol.* **58**, 1233–1258 (1987).
32. Reynolds, J. H. & Heeger, D. J. The Normalization Model of Attention. *Neuron* **61**, 168–185 (2009).
33. Dayan, P. & Abbott, L. *Theoretical Neuroscience: Computational and Mathematical Modeling of Neural Systems*. (The MIT Press, 2001).
34. Montijn, J. S., Klink, P. C. & van Wezel, R. J. A. Divisive Normalization and Neuronal Oscillations in a Single Hierarchical Framework of Selective Visual Attention. *Front. Neural Circuits* **6**, (2012).

35. Deco, G. & Rolls, E. T. A Neurodynamical cortical model of visual attention and invariant object recognition. *Vision Res.* **44**, 621–642 (2004).
36. Gavornik, J. P. & Bear, M. F. Learned spatiotemporal sequence recognition and prediction in primary visual cortex. *Nat. Neurosci.* **17**, 732–737 (2014).
37. Field, D. J. What Is the Goal of Sensory Coding? *Neural Comput.* **6**, 559–601 (1994).
38. Froudarakis, E. *et al.* Population code in mouse V1 facilitates readout of natural scenes through increased sparseness. *Nat. Neurosci.* **17**, 851–857 (2014).
39. Beck, J. M. *et al.* Probabilistic Population Codes for Bayesian Decision Making. *Neuron* **60**, 1142–1152 (2008).
40. Miller, J. K., Ayzenshtat, I., Carrillo-Reid, L. & Yuste, R. Visual stimuli recruit intrinsically generated cortical ensembles. *Proc. Natl. Acad. Sci.* **111**, E4053–E4061 (2014).
41. Barth, A. L. & Poulet, J. F. A. Experimental evidence for sparse firing in the neocortex. *Trends Neurosci.* **35**, 345–355 (2012).
42. Metherate, R., Cox, C. L. & Ashe, J. H. Cellular bases of neocortical activation: modulation of neural oscillations by the nucleus basalis and endogenous acetylcholine. *J. Neurosci.* **12**, 4701–4711 (1992).
43. Pinto, L. *et al.* Fast modulation of visual perception by basal forebrain cholinergic neurons. *Nat. Neurosci.* **16**, 1857–1863 (2013).
44. Coull, J. T., Jones, M. E. P., Egan, T. D., Frith, C. D. & Maze, M. Attentional effects of noradrenaline vary with arousal level: selective activation of thalamic pulvinar in humans. *NeuroImage* **22**, 315–322 (2004).
45. Fries, P. Neuronal Gamma-Band Synchronization as a Fundamental Process in Cortical Computation. *Annu. Rev. Neurosci.* **32**, 209–224 (2009).

46. Börgers, C., Epstein, S. & Kopell, N. J. Gamma oscillations mediate stimulus competition and attentional selection in a cortical network model. *Proc. Natl. Acad. Sci.* **105**, 18023–18028 (2008).
47. Bosman, C. A., Lansink, C. S. & Pennartz, C. M. A. Functions of gamma-band synchronization in cognition: from single circuits to functional diversity across cortical and subcortical systems. *Eur. J. Neurosci.* **39**, 1982–1999 (2014).
48. Goltstein, P. M., Coffey, E. B. J., Roelfsema, P. R. & Pennartz, C. M. A. In Vivo Two-Photon Ca²⁺ Imaging Reveals Selective Reward Effects on Stimulus-Specific Assemblies in Mouse Visual Cortex. *J. Neurosci.* **33**, 11540–11555 (2013).
49. Guizar-Sicairos, M., Thurman, S. T. & Fienup, J. R. Efficient subpixel image registration algorithms. *Opt. Lett.* **33**, 156–158 (2008).
50. Andermann, M. L., Kerlin, A. M., Roumis, D. K., Glickfeld, L. L. & Reid, R. C. Functional specialization of mouse higher visual cortical areas. *Neuron* **72**, 1025–1039 (2011).

Supplementary Information is linked to the online version of the paper at www.nature.com/nature.

Acknowledgements We thank all members of the Cognitive & Systems Neuroscience group for feedback on earlier versions of the manuscript and fruitful discussions, in particular Q. Perrenoud and G. Meijer. We would also like to thank W. Oldenhof, J. Verharen and L. Forsman for assistance with training the animals. This work was supported by the Netherlands Organization for Scientific Research-Excellence grant for the Brain & Cognition project 433-09-208 and the EU FP7-ICT grant 270108.

Author Contributions J.S.M. and P.M.G. built the setup. J.S.M. and C.M.A.P. designed the experiments. J.S.M. performed the experiments and analysed the data. J.S.M. and C.M.A.P. interpreted the results and wrote the paper.

Author Information Reprints and permissions information is available at www.nature.com/reprints. The authors declare no competing financial interests. Correspondence and requests for materials should be addressed to C.M.A.P. (c.m.a.pennartz@uva.nl) or to J.S.M. (j.s.montijn@uva.nl).

Figure legends

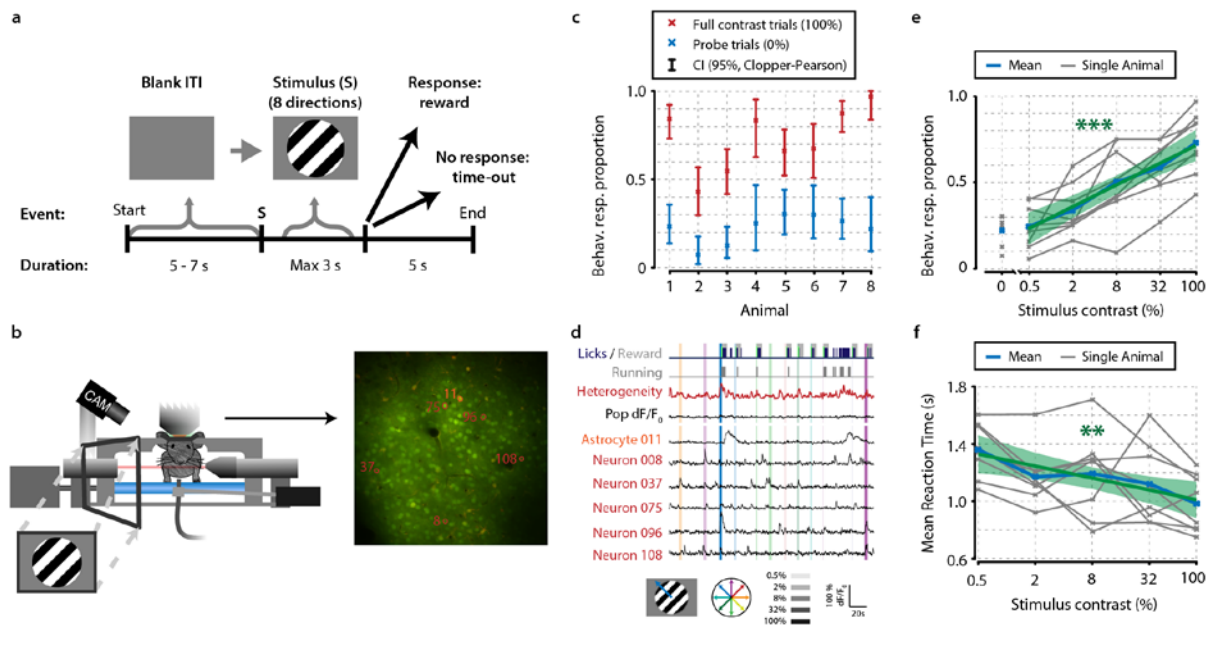


Figure 1. Mice perform a go/no-go task during *in vivo* calcium imaging. **a**, Task schematic showing the time course of a single trial. In each trial, one of a combination of eight different directions and five contrasts, or a probe trial (isoluminant grey blank screen), was presented (ratio 1:5 of probe:stimulus trials). When mice made a licking response during stimulus presentation the visual stimulus was turned off and sugar water was presented. **b**, Schematic of experimental setup. During task performance we recorded eye movements with an infrared sensitive camera, licking responses and running on a treadmill. **c**, All eight animals performed statistically significant stimulus detection during neural recordings, as quantified by non-overlapping 95% Clopper-Pearson confidence intervals ($p < 0.05$) of behavioural response proportions for probe trials and full contrast trials. **d**, Example of simultaneously recorded behavioural measures, population heterogeneity, mean population dF/F_0 , and traces of neurons labelled in panel **b**. Vertical bars represent stimulus presentations; width, colour and saturation represent duration, orientation, and contrast respectively. **e,f**, Animals showed significant increases in behavioural response (behav. resp.) proportion (linear regression analysis, see Supplementary Methods, $p < 0.001$) (**e**) and reductions in reaction time $p < 0.01$)

(f) with higher stimulus contrasts. All panels: Asterisks indicate statistical significance; **
p<0.01; *** p<0.001.

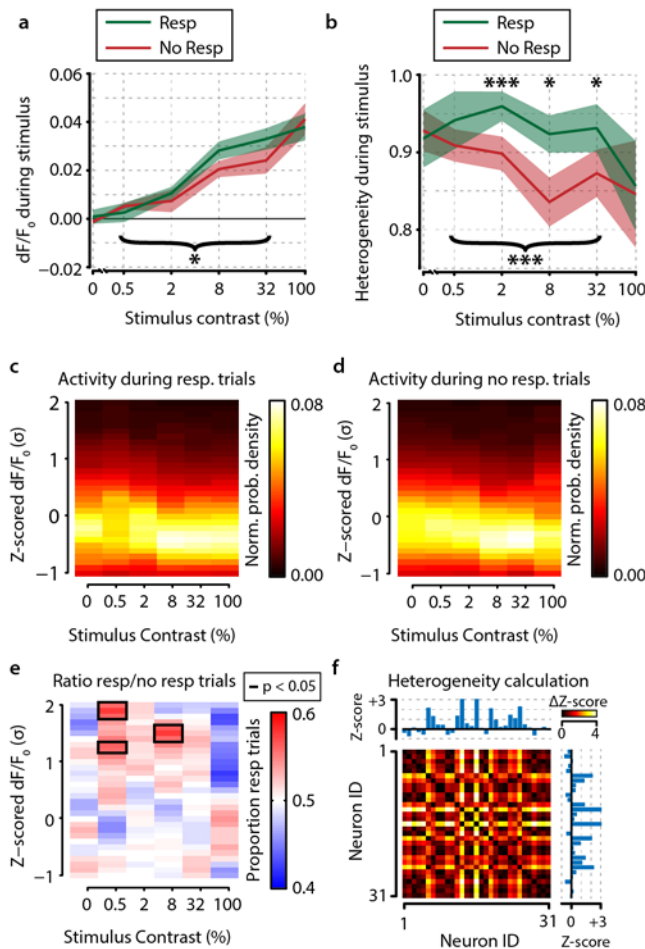


Figure 2. Neural correlates of perceptual decisions reside in the relative activation of subsets of neurons rather than mean activity levels of the population as a whole. **a**, Mean preferred population activity as a function of stimulus contrast shows small differences between response (resp.) and no-response trials (paired t-test on intermediate contrasts 0.5% - 32%, $n=8$ animals, $p<0.05$; individual comparisons, FDR-corrected t-tests; 0% - 100%, $p>0.05$). **b**, Population activity heterogeneity (see **f**) shows much stronger correlations with visual detection than mean population activity (see **a**; measure of effect size analysis, $p<0.05$). Comparison between response and no-response trials for intermediate contrasts (paired t-test, $p<0.001$) as well as some individual contrasts (FDR-corrected paired t-tests; 0%, $p=0.781$; 0.5%, $p=0.424$; 2%, $p<0.001$; 8%, $p<0.05$; 32%, $p<0.05$; 100%, $p=0.758$) reached significance. **c,d**, Normalized probability density of z-scored dF/F_0 during response (**c**) and

no-response (**d**) trials for different contrasts. **e**, Ratio of the normalized dF/F0 amplitudes during response (**c**) over no-response (**d**) trials shows differences in the shape of neuronal response distributions. During response trials, subsets of neurons with higher activity levels are overrepresented, indicating an increase in skewness of the population activity distributions. Bins enclosed by black lines are statistically significantly higher than expected by chance (shuffling analysis, see Online Methods, $p < 0.05$). **f**, Schematic representation of the method to compute heterogeneity on an example trial (see also Online Methods). The dF/F0 response of each neuron is z-scored per contrast and the distance (absolute difference) in z-scored activity between all pairs of neurons is calculated for each trial (color-coded ΔZ -score). The population heterogeneity in a given trial is defined as the mean ΔZ -score over all neuronal pairs. All panels: Asterisks indicate statistical significance; * $p < 0.05$; *** $p < 0.001$.

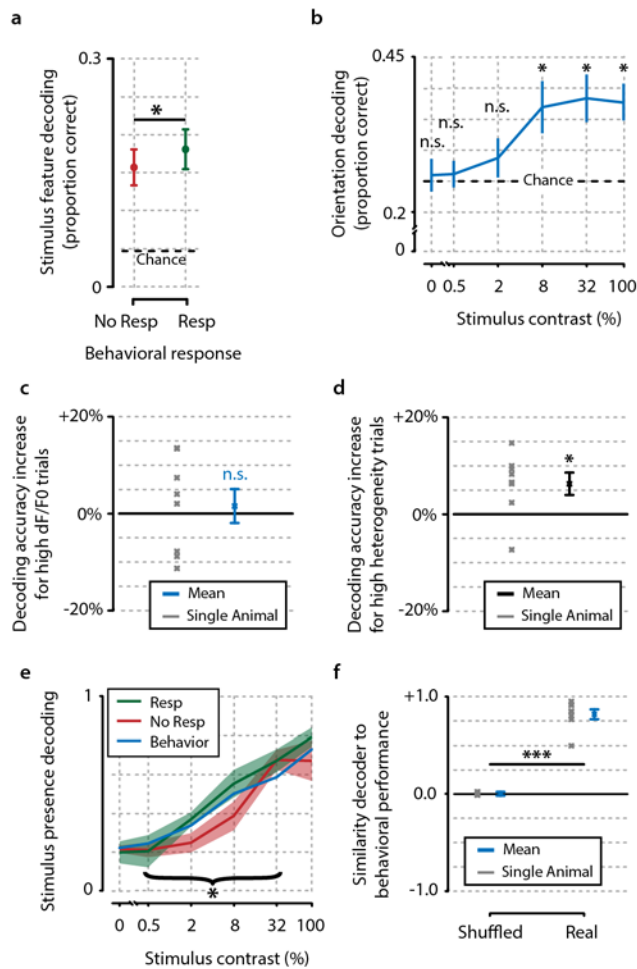


Figure 3. Fidelity of stimulus representation (orientation, contrast) and population heterogeneity are intimately linked to accurate visual detection. **a**, Analysis with a Bayesian Maximum-Likelihood (ML) decoder shows that during hit trials stimulus features are more accurately represented in the population response pattern than during miss trials (paired t-test, $n=8$ animals, $p<0.05$). **b**, Orientation decoding as a function of stimulus contrast shows a sigmoid curve. Statistical analysis revealed significantly above-chance orientation decoding for contrasts higher than 2% (post hoc FDR-corrected one-sample t-tests vs chance level (25%; four orientations were used); 0%, $p=0.724$; 0.5, $p=0.721$; 2%, $p=0.410$; 8%, $p<0.05$; 32%, $p<0.05$, 100%, $p<0.05$). **c,d**, Orientation decoding accuracy does not increase when only strong responses to stimuli are taken into account (**c**, one-sample t-test, $p=0.669$), but does increase for high population heterogeneity (**d**, $p<0.05$). **e**, Decoding of stimulus presence (see

Online Materials) shows similar accuracy as actual behavioural performance by the animals (see also fig. 1e). When the animal is making a correct judgment about stimulus presence (resp; green line), the decoder is also better able to correctly judge its presence (paired t-test over intermediate contrasts, $p < 0.05$). **f**, Behavioural stimulus detection performance is more similar to the optimal decoder's performance than expected by chance (paired t-test, $n = 8$ animals, shuffled vs. real similarity, $p < 0.001$). All panels: Asterisks indicate statistical significance; * $p < 0.05$; *** $p < 0.001$.

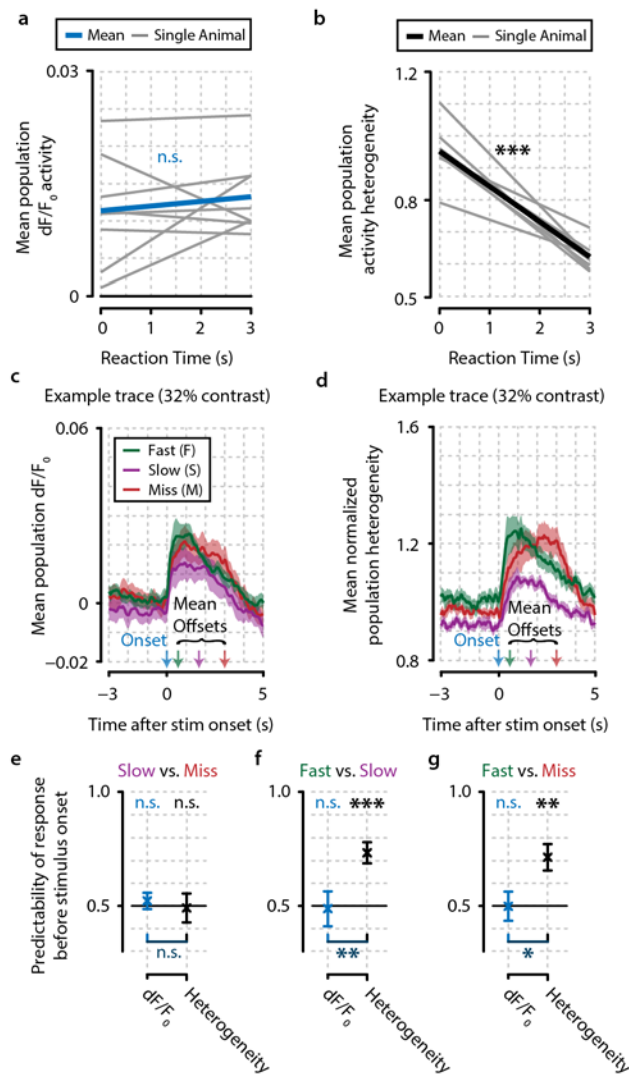


Figure 4. Heterogeneity is correlated with reaction time. **a,b**, Reaction time shows no correlation with mean dF/F_0 activity during stimulus presentation (FDR-corrected one sample t-test over individual regression slopes per animal, $n=8$, n.s.) but a strong correlation with heterogeneity ($p < 0.001$). **c,d**, Example traces for population dF/F_0 and heterogeneity for fast (F, green), slow (S, yellow) and miss (M, red) responses (mean \pm st. error over animals) also showing mean stimulus offsets. **e-g**, Behaviourally fast responses are predictable before stimulus onset using heterogeneity (FDR-corrected one-sample t-tests vs chance level (0.5); **e**, S-M, $p=0.799$; **f**, F-S, $p < 0.001$; **g**, F-M, $p < 0.01$), but not using dF/F_0 (FDR-corrected one-sample t-tests vs chance level; **e**, S-M, $p=0.157$; **f**, F-S, $p=0.811$; **g**, F-M, $p=0.924$; FDR-

corrected paired t-test for heterogeneity vs $dF/F0$; **e**, S-M, $p=0.477$; **f**, S-F, $p<0.01$; **g**, F-M, $p<0.05$). All panels: Asterisks indicate statistical significance; * $p<0.05$; ** $p<0.01$; *** $p<0.001$.

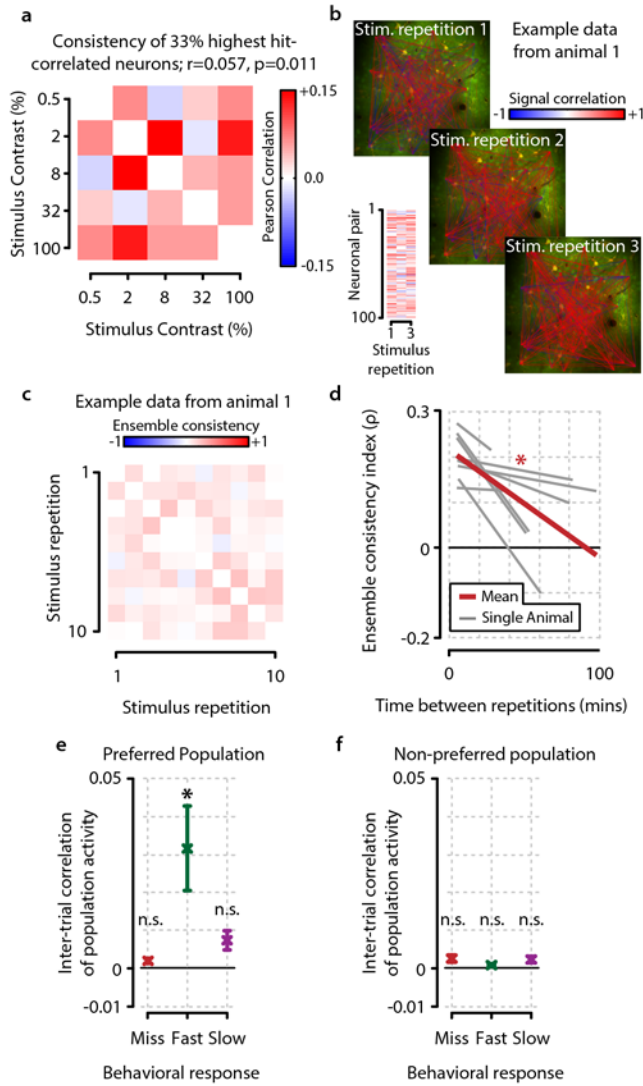
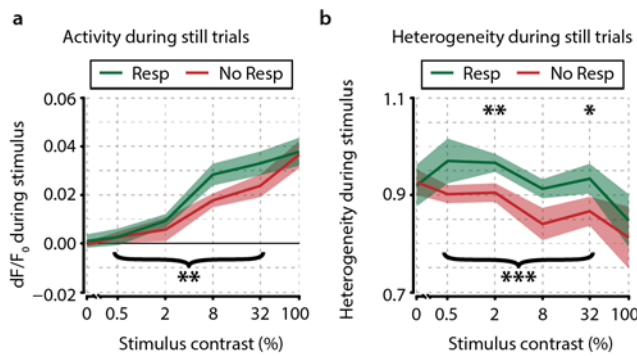


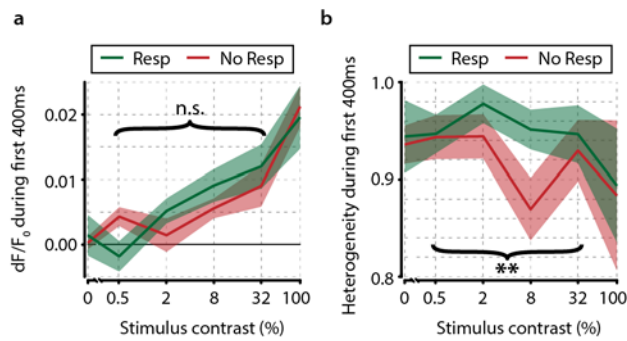
Figure 5. Consistency of stimulus-evoked population activity is specifically increased during fast behavioural responses and decreases over time. **a**, Analysis of the consistency of the 33% highest hit-correlated neurons shows a low ($r=0.057$), but significantly above-zero consistency when computed over different stimulus contrasts (one-sample t-test, $p<0.05$); indicating that some neurons reproducibly increase their activity during hit trials. **b**, Graphical depiction of neuronal pairwise signal correlations per stimulus repetition. **c**, Example inter-repetition population code consistency, from same animal as **b**. **d**, Quantification of ensemble consistency, showing a significant decrease of population code similarity over time (one-sample t-test over individual regression slopes per animal, $n=8$,

p<0.05). **e,f**, Inter-trial correlations as quantification of ensemble reoccurrence are significantly different from zero only during fast behavioural response trials and only within the preferred neuronal population (FDR-corrected one-sample t-tests vs 0, preferred population; miss, p=0.791; fast, p<0.05; slow, p=0.303; non-preferred population; miss, p=0.356; fast, p=0.809; slow, p=0.618). Error bars indicate the standard error of the mean. All panels: Asterisks indicate statistical significance; * p<0.05.

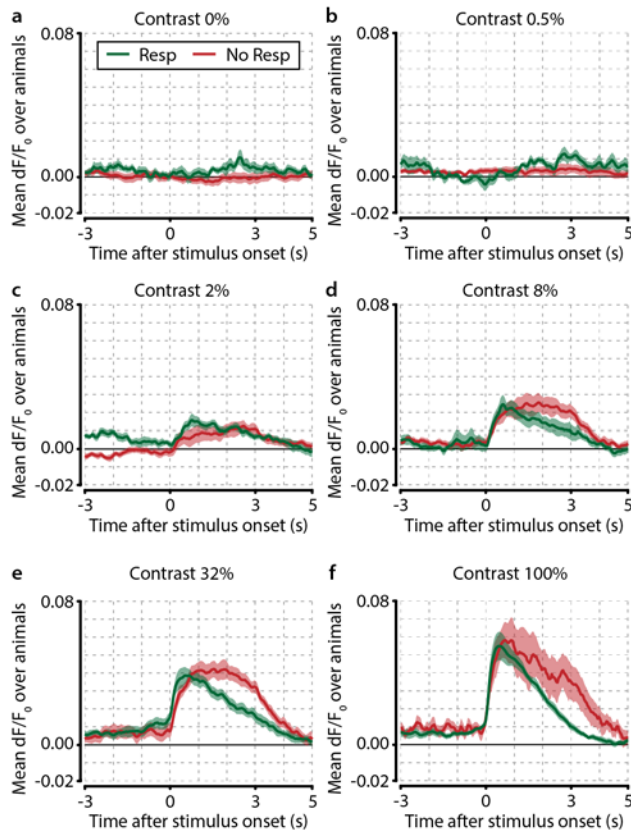
Extended data figure legends



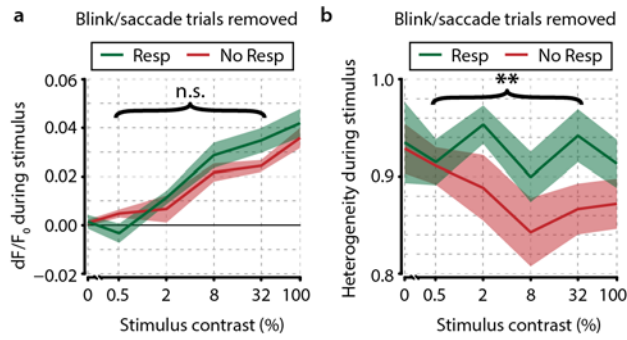
Extended Data Figure 1. Removal of locomotion trials does not qualitatively affect neural correlates of stimulus detection. **a**, When computed only on trials where animals were not moving (89.9% of trials), the mean population dF/F₀ as a function of stimulus contrast shows little difference with the original analysis (compare to fig. 2a). FDR-corrected statistics showed no significant differences for any individual contrast (0%, p=0.530; 0.5%, p=0.983; 2%, p=0.353; 8%, p=0.060; 32%, p=0.065; 100%, p=0.777). Paired t-test over intermediate contrasts (0.5%-32%) showed a significant difference between response and no-response trials (p<0.05). Our original results are very similar to the current analyses and are therefore not dependent on movement-induced modulations. **b**, As **a**, but for heterogeneity (still trials only); single contrast FDR-corrected t-tests were slightly less significant than the original analysis (0%, p=0.859; 0.5%, p=0.189; 2%, p<0.005; 8%, p=0.122; 32%, p<0.05; 100%, p=0.195), but were overall quite similar to fig. 2b. The overall paired t-test for hit/miss differences grouping 0.5% - 32% contrasts was also still highly significant (p<0.001), suggesting that our main results are not due to locomotion-related artefacts. All panels: asterisks indicate statistical significance; * p<0.05; ** p<0.005; *** p<0.001.



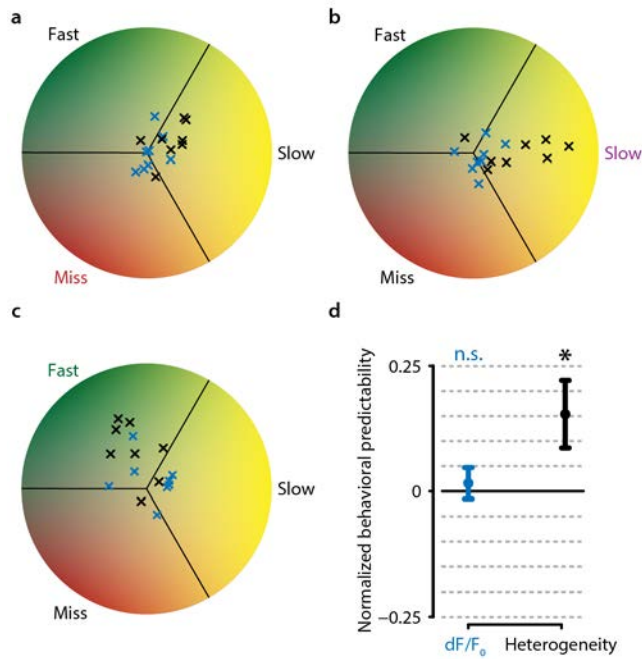
Extended Data Figure 2. Population correlates of visual detection are not dependent on motor-related signals. **a**, As fig. 2a; mean population dF/F_0 as a function of contrast, now using only the first ~400 ms (394 ms; 10 frames) after stimulus onset. Mean reaction time over animals and contrasts was ~1.2s (see fig. 1f), leaving on average about 0.8s between the last data point included in this analysis and the subsequent licking response. Note the absence of any neuronal activity during responses to probe trials (green line, 0% contrast, t-test vs. 0, $p=0.549$). **b**, As **a**, but for heterogeneity (compare with fig. 2b). Results were qualitatively similar to our original analysis for heterogeneity, but not for dF/F_0 (paired t-test over intermediate contrasts for dF/F_0 , $p=0.543$, for heterogeneity, **, $p<0.01$).



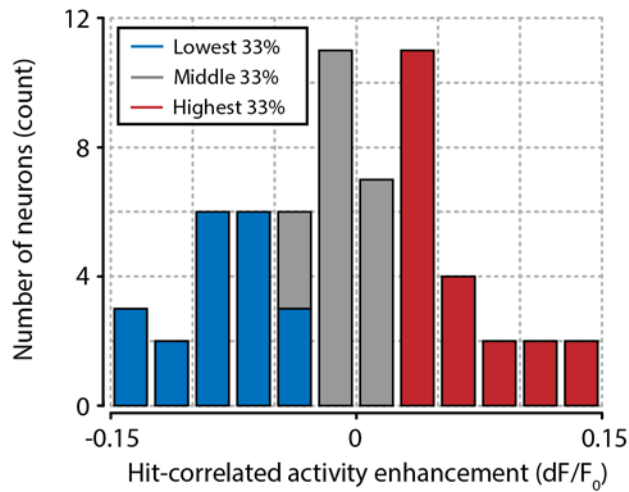
Extended Data Figure 3. Traces of population dF/F_0 averaged over animals ($n=8$) for different contrasts show the difference between response and no-response trials over time. **a**, probe trials (0% stimulus contrast). **b**, 0.5% contrast. **c**, 2% contrast. **d**, 8% contrast. **e**, 32% contrast. **f**, 100% contrast. Response trials (green) show quicker offsets, because the stimulus turns off when the animal makes a licking response. Also note the absence of any motor-related activity in panel **a**, supporting the interpretation that the observed correlates are unrelated to motor activity or preparation.



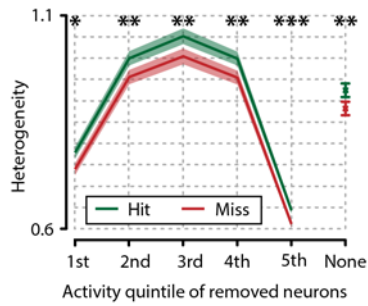
Extended Data Figure 4. Population correlates are not explained by eye blinks or saccades. **a**, As fig. 2a; mean population dF/F_0 as a function of contrast, using only trials in which the animal's eye position remained fixed and no blinks were detected during the entire stimulus period. **b**, As **a**, but for heterogeneity (compare with fig. 2b). Our results are qualitatively and quantitatively similar for heterogeneity; paired t-test over intermediate contrasts revealed a significant difference between response and no-response trials (**, $p < 0.005$), but not for dF/F_0 ($p = 0.136$).



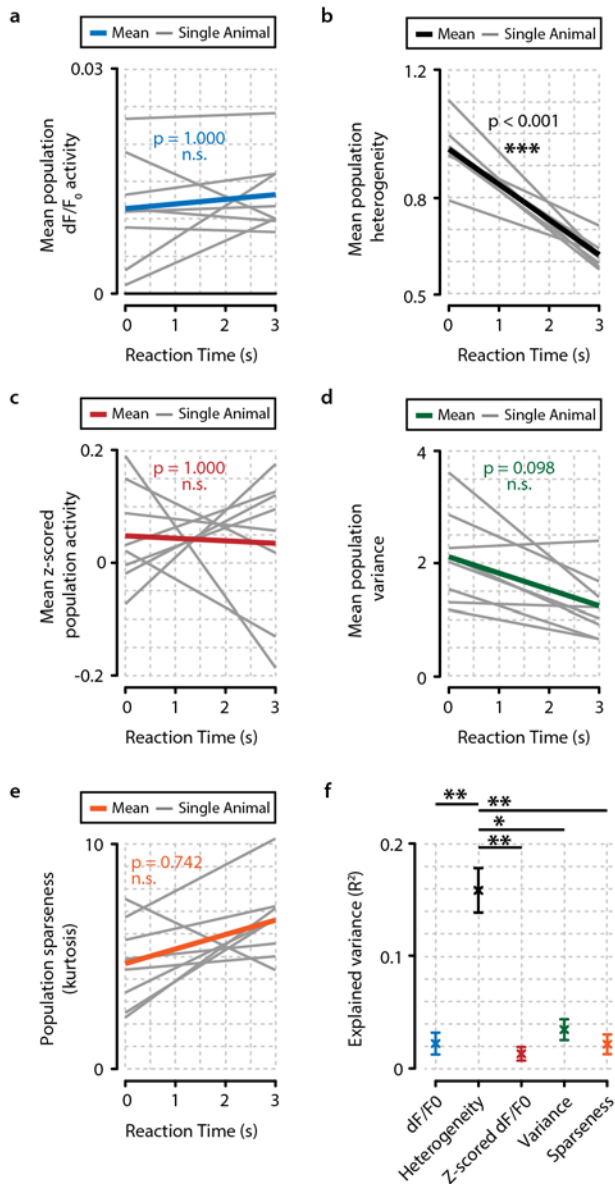
Extended Data Figure 5. Behavioural response is predictable on single trials when using heterogeneity, but not when using dF/F_0 . **a**, Predictive decoding of miss trials using mean population dF/F_0 (blue) or heterogeneity (black) during 3s preceding stimulus onset. Each point is the mean prediction for a single animal (see Supplementary Methods). **b**, same as **a**, but for slow trials. **c**, same as **a**, but for fast trials. **d**, Quantification of predictability shows chance-level prediction using dF/F_0 (one-sample t-test, $p=0.661$), but above-chance prediction of behavioural responses using heterogeneity ($p<0.05$). Single points at left are single animal/response-type combinations ($n=3$ points / animal). Point with error bars at right are mean \pm standard error ($n=24$).



Extended Data Figure 6. Schematic shows example from one recording of splitting neuronal populations in thirds of neurons showing an enhanced response on hit relative to miss trials. All neurons are sorted by the increase in dF/F_0 from no-response to response trials for a single contrast. The 33% with the highest difference is defined as the group of hit-correlated neurons used for further analysis.

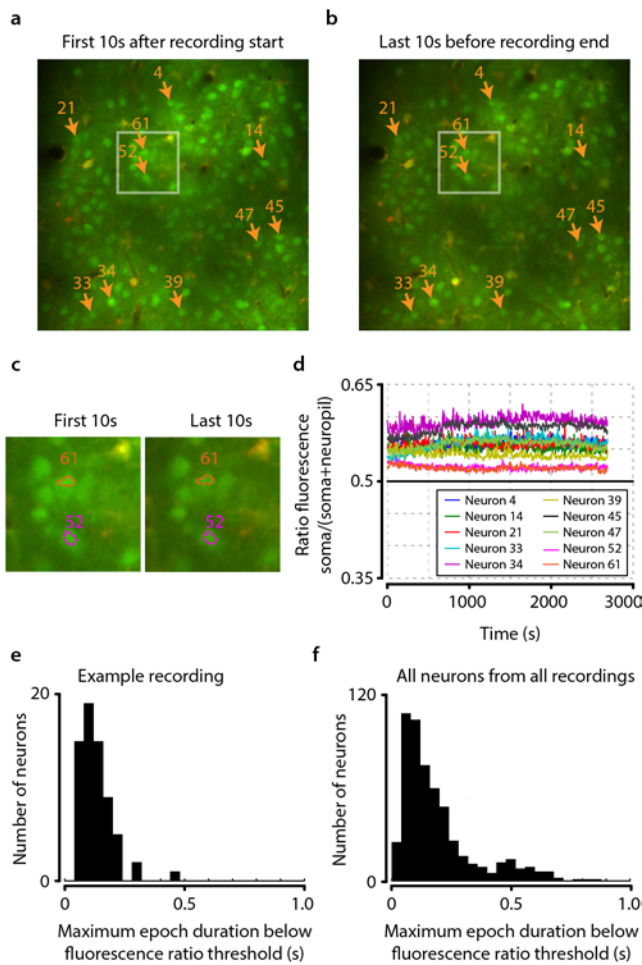


Extended Data Figure 7. Difference in heterogeneity between hit and miss trials is a population-distributed process and does not critically depend on selecting the most, or least, active neurons. On a single-trial basis we removed a single quintile of neurons within a z-scored activity bracket and recalculated the hit/miss difference after removal of this quintile (see Online Methods). While removal of the least (1st quintile) or most (5th quintile) active neurons per trial led to a decrease in absolute heterogeneity, the differences between hit and miss trials remained intact (paired t-tests hit vs. miss, n=8, 1st quintile $p < 0.05$, 2nd $p < 0.005$, 3rd $p < 0.005$, 4th $p < 0.005$, 5th $p < 0.001$, no removal $p < 0.005$). Data show mean and standard error over animals (n=8). Asterisks indicate statistical significance; * $p < 0.05$; ** $p < 0.005$; *** $p < 0.001$.



Extended Data Figure 8. Relationships between reaction-time (RT) and dF/F₀, heterogeneity, z-scored activation and variance show that only heterogeneity correlates with behavioural performance. **a**, dF/F₀ plotted as a function of RT (Bonferroni-Holmes corrected one-sample t-test of slopes vs. 0, $p=1.000$). **b**, as **a**, but for heterogeneity ($p<0.001$). **c**, as **a**, but for z-scored dF/F₀ ($p=1.000$). **d**, as **a**, but for variance ($p=0.098$). **e**, as **a**, but for population sparseness ($p=0.742$). **f**, Explained variance (R^2) of single trial population responses as a function of RT for the five different measures plotted as mean +/- standard error over animals. Heterogeneity explains significantly more variance than any of the four other measures

(Bonferroni-Holmes corrected paired t-test, heterogeneity vs. dF/F0, $p < 0.01$; vs. z-scored dF/F0, $p < 0.01$; vs. variance, $p < 0.05$; vs. sparseness, $p < 0.01$). None of the other four metrics differed significantly in R^2 from each other (t-tests, n.s.). All panels: Asterisks indicate statistical significance; * $p < 0.05$; ** $p < 0.01$; *** $p < 0.001$.



Extended Data Figure 9. Neuronal signals are stable over time in all recordings. **a,b**, example from one animal showing the average of all recorded frames during the first 10 seconds after imaging onset (**a**) and during the last 10 seconds before the end of the recording (**b**). The locations of 10 randomly selected neurons are marked by orange arrows, and the white coloured rectangles depict the area enlarged in panel **c**. **c**, enlarged subsection of the images shown in **a** and **b**, showing the outlines of cells 52 and 61. Note the similarity of the cell bodies and their outlines. **d**, down-sampled traces showing the ratio of soma vs. neuropil fluorescence of the 10 randomly selected neurons shown in panels **a** and **b** over duration of the entire recording (see Supplementary Methods). All traces remain above the equiluminance threshold of 0.5, indicating that these neurons' somata remain visible and do not disappear due to bleaching or slow z-drift. **e**, histogram showing the maximum epoch duration of

dropping below the equiluminance threshold of 0.5 for all neurons from the example session. None of the cells remain undetectable for longer than 0.5 seconds. **f**, as **e**, but for all cells from all recordings. Again, none of the cells have a prolonged period (>1.0 second) of being undetectable, indicating robust stability of the neuronal signals over time.